Global Biogeochemical Cycles

RESEARCH ARTICLE
10.1029/2017GB005856

Key Points:
- Central and Northern European forest growth is expected to benefit (suffer) from additional warming in regions with a mean growing season temperature below (above) 15.9 plus-minus 1.4 degrees Celsius
- A vegetation model ensemble mean agrees with this threshold but is too sensitive to temperature changes at coldest and warmest locations
- Model improvements are needed to predict forest growth more accurately and guide silvicultural practices

Supporting Information:
- Supporting Information S1
- Table S1

Correspondence to:
S. Klesse,
sklesse@email.arizona.edu

Citation:
Klesse, S., Babst, F., Lienert, S., Spahni, R., Joos, F., Bouriaud, O., et al. (2018). A combined tree ring and vegetation model assessment of European forest growth sensitivity to interannual climate variability. *Global Biogeochemical Cycles*, *32*. https://doi.org/10.1029/2017GB005856

Received 5 DEC 2017
Accepted 21 JUL 2018
Accepted article online 30 JUL 2018

A Combined Tree Ring and Vegetation Model Assessment of European Forest Growth Sensitivity to Interannual Climate Variability

S. Klesse[1,2,3], F. Babst[1,3,4], S. Lienert[2,5], R. Spahni[2,5], F. Joos[2,5], O. Bouriaud[6,7], M. Carrer[8], A. Di Filippo[9], B. Poulter[10], V. Trotsiuk[1,11,12], R. Wilson[13,14], and D. C. Frank[1,2,3]

[1]Swiss Federal Institute of Forest, Snow and Landscape Research (WSL), Birmensdorf, Switzerland, [2]Oeschger Centre for Climate Change Research, Bern, Switzerland, [3]Laboratory of Tree-Ring Research, University of Arizona, Tucson, AZ, USA, [4]Department of Ecology, W. Szafer Institute of Botany, Polish Academy of Sciences, Krakow, Poland, [5]Climate and Environmental Physics, Physics Institute, University of Bern, Bern, Switzerland, [6]National Institute for Research-Development in Forestry, National Forest Inventory, Voluntari, Romania, [7]Integrated Center for Research, Development and Innovation in Advanced Materials, Nanotechnologies, and Distributed Systems for Fabrication and Control, Stefan cel Mare University of Suceava, Suceava, Romania, [8]Dipartimento Territorio e Sistemi Agro-Forestali, Università degli Studi di Padova, Legnaro, Italy, [9]Department of Agriculture and Forestry ScieNcE, Università della Tuscia, Viterbo, Italy, [10]NASA GSFC, Biospheric Sciences Laboratory, Greenbelt, MD, USA, [11]Faculty of Forestry and Wood Sciences, Czech University of Life Sciences Prague, Prague, Czech Republic, [12]Institute of Agricultural Sciences, Zurich, Switzerland, [13]School of Earth and Environmental Sciences, University of St Andrews, Saint Andrews, UK, [14]Lamont-Doherty Earth Observatory, Columbia University, Palisades, NY, USA

Abstract The response of forest growth to climate variability varies along environmental gradients. A growth increase and decrease with warming is usually observed in cold-humid and warm-dry regions, respectively. However, it remains poorly known where the sign of these temperature effects switches. Here we introduce a newly developed European tree ring network that has been specifically collected to reconstruct forest aboveground biomass increment (ABI). We quantify, how the long-term (1910–2009) interannual variability of ABI depends on local mean May–August temperature and test, if a dynamic global vegetation model ensemble reflects the resulting patterns. We find that sites at 8 °C mean May–August temperature increase ABI on average by 5.7 ± 1.3%, whereas sites at 20 °C decrease ABI by 3.0 ± 1.8% m^{-2} $year^{-1}$ $\Delta°C^{-1}$. A threshold temperature between beneficial and detrimental effects of warming and the associated increase in water demand on tree growth emerged at 15.9 ± 1.4 °C mean May–August temperature. Because interannual variability increases proportionally with mean growth rate—that is, the coefficient of variation stays constant—we were able to validate these findings with a much larger tree ring data set that had been established following classic dendrochronological sampling schemes. While the observed climate sensitivity pattern is well reflected in the dynamic global vegetation model ensemble, there is a large spread of threshold temperatures between the individual models. Also, individual models disagree strongly on the magnitude of climate impact at the coldest and warmest locations, suggesting where model improvement is most needed to more accurately predict forest growth and effectively guide silvicultural practices.

1. Introduction

The fifth phase of the Coupled Model Intercomparison Project projects a 63 ± 27% increase in global Net Primary Productivity (NPP) by 2099 under the *business-as-usual* CO_2 emissions scenario (Representative Concentration Pathway 8.5 (RCP8.5); Wieder et al., 2015), integrating the terrestrial response to a variety of physiological, ecological, and climatic processes. Rising atmospheric CO_2 concentration is generally expected to increase plant growth (Iversen & Norby, 2014). This increase can be further enhanced by increasing temperatures and longer growing seasons (Churkina et al., 2005) or alternatively be offset through water stress induced by increased evaporative demand (Williams et al., 2013). Similarly, variation in nutrient availability (Fatichi et al., 2014), management strategy (Noormets et al., 2015; Rydval et al., 2015), and disturbance frequency and intensity, such as insect outbreaks or storm damages (Seidl et al., 2014), are known to impact the terrestrial land carbon sink. These interacting terms determine the annual residual terrestrial carbon balance, which has varied from a 0.45 Pg C/year source to a 4.03 Pg C/year sink during the past 50 years (Le Quéré et al., 2015). These

values are inferred as the net difference between the sum of emissions by fossil fuel combustion and land cover change and the CO_2 uptake by the atmosphere (i.e., the annual growth rate of CO_2 concentration) and ocean. The aggregated sink values are, however, based on average biome-specific responses to environmental forcing and characterized by high variability and uncertainties concerning temporal dynamics and spatial manifestations (Nemani, 2003; Piao et al., 2013; Poulter et al., 2014; Reichstein et al., 2013).

Quantifying the sensitivity of individual biomes to environmental variation is thus crucial to anticipate their fates under future climate. This challenge has been addressed by diverse approaches including repeated field measurements (Clark et al., 2001), climate manipulation experiments, satellite (Nemani, 2003), and eddy-covariance data (Beer et al., 2010), together with subsequent integration into biogeochemical and Earth System Models (Medlyn et al., 2015). However, synthesizing observations into quantitative constraints of ecosystem responses to environmental changes is challenged by a lack of high-temporal resolution (forest inventories), indirect measures of plant carbon uptake (satellite data), or short time series (eddy covariance and climate manipulation experiments). In this study, we take advantage of a long-term, annually resolved, spatially extensive, and in situ data source that enables us to quantify the absolute climate sensitivity (i.e., gram carbon per year per square meter per degree Celsius) and interannual variability of aboveground forest growth: Tree ring networks provide useful records of how mean climate conditions control tree growth responses to annually varying climatic parameters (Babst et al., 2013; St. George, 2014; Vicente-Serrano et al., 2014; Williams et al., 2010). Yet most tree ring studies report only the direction and strength of a climate-growth relationship (correlation coefficient) and leave the actual degree to which the climatic driver affects tree growth unaddressed. However, this sensitivity estimate (regression slope), which is a result of tree growth variability and the strength of the climate-growth relationship, would be necessary to be able to determine the magnitude of climate change impact on current and future tree growth.

In this study we introduce a new tree ring network comprising 49 sites and spanning a large climate gradient across Europe that—in contrast to most available tree ring data sets—has been specifically collected with a sampling scheme designed to reconstruct forest aboveground biomass increment (ABI, Figures 1a and 1b; Babst, Bouriaud, Alexander, et al., 2014; Davis et al., 2009; Nehrbass-Ahles et al., 2014). We use this new tree ring network to (i) quantify the interannual variability of ABI across European forest ecosystems and (ii) assess the interannual climate sensitivity of European forest growth. Additionally, we compare our results to data from a publicly available tree ring data set (Babst et al., 2013) to evaluate the influence of two different standardization and sampling methods on growth variability and climate sensitivity in Europe. Further, we use the observed pattern of climate sensitivity to benchmark NPP estimates from a dynamic global vegetation model (DGVM) ensemble that has been frequently used in global carbon cycle analyses (TRENDY, Sitch et al., 2015).

2. Materials and Methods

2.1. Study Area and Sampling Design

We employed a fixed-plot sampling design (Babst, Bouriaud, Alexander, et al., 2014) where all tree individuals (alive, dead standing and lying, and stumps) with a diameter at breast height $>$5.6 cm were sampled (Table S1 in the supporting information). We recorded the position, height, and diameter at breast height of each tree before collecting two increment cores parallel to the slope, as well as stem discs of the dead trees (where applicable). We sampled 40 plots across Europe between 2012 and 2014 (Figure 1b) along a climate gradient ranging from 7.5 to 21.2 °C May, June, July, and August (MJJA) temperature and 85 to 690 mm of MJJA precipitation (1980–2009, Figure 1a). Eight additional sites from Babst, Bouriaud, Alexander, et al. (2014) and one site from Nehrbass-Ahles et al. (2014) were included leading to a total of 49 sites. Plot selection focused on two of the most abundant and important tree species in Europe spruce (*Picea abies*) and beech (*Fagus sylvatica*, San-Miguel-Ayanz et al., 2016, Mauri et al., 2017), but other species such as larch (*Larix decidua*), fir (*Abies alba*), and pine (*Pinus sylvestris* and others) were also included. Stand compositions range from monocultures to mixed forests and from young plantations (~50 years old) to old-growth multilayered stands (see Table S1).

2.2. Tree Ring Data

Tree cores were prepared and measured using standard dendrochronological techniques. Missing rings and distance to pith were estimated as in Nehrbass-Ahles et al. (2014), and the transformation from one-dimensional tree ring width series to individual ABI followed Babst, Bouriaud, Alexander, et al. (2014).

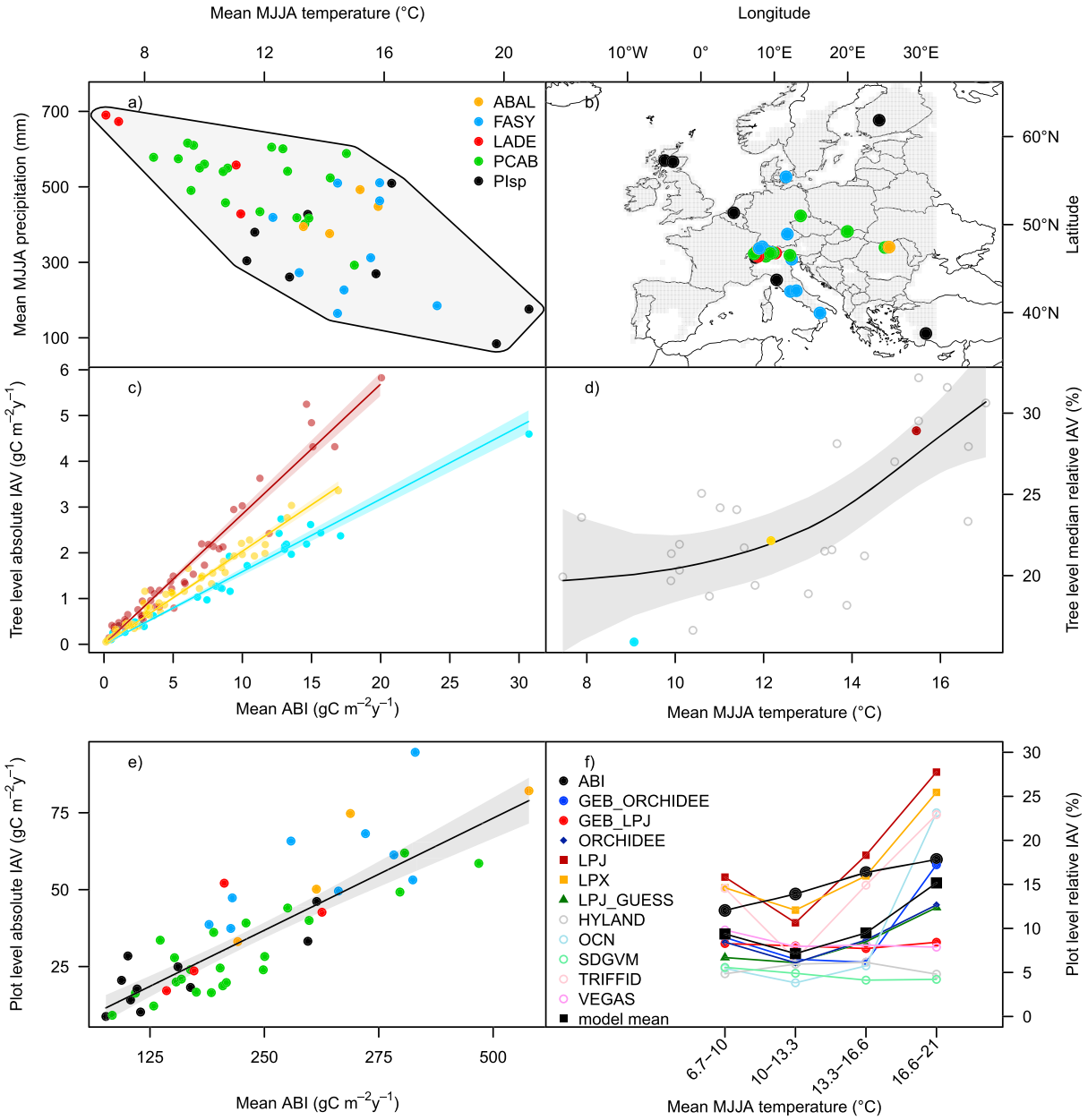

Figure 1. Climatic (a) and spatial (b) domain of the tree ring network, (c) relationship between absolute IAV and mean ABI of individual *Picea abies* trees at three exemplary plots for 1980–2009, which were chosen to represent each one site with low, medium, and high IAV, where all size classes are represented evenly, (d) relationship between median relative IAV of *Picea abies* trees at plots with $n > 6$ *Picea abies* trees and mean growing season temperature, (e) relationship between absolute IAV and mean ABI for 1980–2009, and (f) median observed and simulated relative IAV for 1980–2009 across four temperature bins. Relative IAV is the coefficient of variation of absolute IAV. Colors in (a, b, and e) refer to different dominant tree species (abbreviations according to International Tree Ring Data Bank, ABAL = *Abies alba*, FASY = *Fagus sylvatica*, LADE = *Larix decidua*, PCAB = *Picea abies*, Plsp = *Pinus* sp. pl. (*P. sylvestris*, *P. pinaster*, and *P. brutia*), that is, the species with the highest basal area percentage at a given site. The gray shaded area in (a) and (b) corresponds to the climate space covered with a buffer of ±0.5 °C temperature and ± 20 mm precipitation. Shadings in (c)–(e) represent the 95% confidence interval of the corresponding regression. IAV = interannual variability; ABI = aboveground biomass increment; MJJA = May, June, July, August.

Up to six suitable species-specific allometric equations were thereby applied to the reconstructed tree diameters in each year to calculate aboveground woody biomass through time (Table S2). ABI was calculated as the year-to-year difference of the sum of all individual tree biomass values and expressed as gram carbon per square meter per year. Interannual variability was calculated over the 1980–2009 period as the mean coefficient of variation of ABI of a running 10-year window. We chose this rather short period because of the increasing uncertainty of the reconstructed stand ABI toward the past (Foster et al., 2014) and to

ensure that the coefficient of variation was not heavily influenced by nonclimatic influences, including influences related to either short-term pulses or longer-term trends caused by management (Davis et al., 2009), natural disturbances, or stand dynamics. In total, we have reconstructed annual ABI, $ABI_i\,(t_{i,j})$, for 49 individual sites with site number i (i = 1:49); each record includes N_i values for years $t_{i,j}$, with j running from the first to the last year of observation of site i.

To facilitate comparisons with gridded DGVM simulations over Europe, we grouped ABI and NPP estimates into four temperature ranges that generally represent (1) high elevation coniferous stands (6.7–10 °C), (2) mixed forests of the montane zone (10–13.3 °C), (3) lowland (13.3–16.6 °C), and (4) Mediterranean forests (16.6–21 °C; see also Figure 1f).

We note that although ABI is not entirely equivalent to total NPP—as it excludes foliage and belowground biomass components (including root symbionts as well as exudates and the production of volatile organic carbon)—empirical studies have shown that ABI is as a valid proxy of NPP as they are highly correlated (Luyssaert et al., 2007, Figure S1).

2.3. Climate Data

Monthly mean temperature and precipitation totals for the site locations were derived by adjusting the CRU TS 3.21 time series (Harris et al., 2014) to the mean climatology of the nearest WorldClim (1 × 1 km, Hijmans et al., 2005) grid cell with a comparable elevation (20 cell search radius). For temperature, absolute anomalies were calculated by subtracting the long-term (1950–2000, corresponding to WorldClim) monthly means from the entire CRU TS 3.21 time series (1901–2013) and relative anomalies were calculated for precipitation (observed precipitation divided by monthly means). These anomalies were added to (or multiplied with, in the case of precipitation) the WorldClim baseline climatology. In this way, we obtain 49 records for monthly mean temperature, $T_i\,(m,t)$, and precipitation, $P_i\,(m,t)$ with index m (m = 1:12) indicating the month of the year and t (t = 1901:2013) the year. The monthly data are averaged over the period MJJA and for each year to get $T_i^{\mathrm{MJJA}}\,(t)$ and $P_i^{\mathrm{MJJA}}\,(t)$.

2.4. Climate Sensitivity Estimation

Next, we estimate the sensitivities of ABI to interannual variations in May to August temperature and precipitation for each site. First, we high-pass filtered the ABI and climate time series with a flexible cubic smoothing spline (50% frequency cutoff at 10 years) to remove multidecadal trends. The aim is to dampen possible nonclimatic influences on ABI variations. Due to this flexible standardization, we do not evaluate trends in absolute ABI and NPP that are codriven by longer-term changes in CO_2 and nitrogen fertilization, stand dynamics and forest management, and land cover. The tree ring data were detrended by division, whereas the climate data were subtracted from the smoothing spline to retain absolute units to which we can refer a relative change in ABI. In the following only detrended data are used. The climate sensitivities (partial regression slopes) of forest growth are determined at each plot through a multiple linear regression such that

$$ABI_i\left(t_{i,j}\right) = s_i^T \cdot T_i^{\mathrm{MJJA}}\left(t_{i,j}\right) + s_i^P \cdot P_i^{\mathrm{MJJA}}\left(t_{i,j}\right) + \varepsilon_i^{\mathrm{ABI}}\left(t_{i,j}\right). \quad (1)$$

$\varepsilon_i^{ABI}\,(t_{i,j})$ represents the deviation between the linear regression fit and an individual measurement of ABI. s_i^T and s_i^P are the sensitivities of ABI to interannual variations in May to August temperature and precipitation, respectively. These sensitivities correspond to the partial derivatives $\frac{\partial ABI_i}{\partial T_i^{\mathrm{MJJA}}}$ (% °C^{-1}) and $\frac{\partial ABI_i}{\partial P_i^{\mathrm{MJJA}}}$(% 100 mm^{-1}). In this way, we obtain 49 pairs (s_i^T, s_i^P) of local, plot-specific climate sensitivity values.

Next, we determine the relationships between the local sensitivities and the large-scale, spatial gradient in climatological mean temperature and precipitation. Forty-nine climatological mean May to August temperature values, $T_i^{\overline{\mathrm{clim}}}$, are computed by averaging the undetrended annual values of $T_i^{\mathrm{MJJA}}\,(t)$ for each site over the period 1910 to 2009. Then, the sensitivities are regressed as follows:

$$s_i^T = rsT^T * T_i^{\overline{\mathrm{clim}}} + \varepsilon_i^T \text{ and} \quad (2)$$

$$s_i^P = rsP^T * T_i^{\overline{\mathrm{clim}}} + \varepsilon_i^P. \quad (3)$$

rsT^T and rsP^T denote the regression coefficients and ε_i^T and ε_i^P denote again the residuals between the fit and local sensitivities. The two new regression coefficients rsT^T and rsP^T provide an estimate how the sensitivities

of ABI to interannual variation in temperature, s_i^T, and precipitation, s_i^P, vary along the climatological gradient in mean May–August temperature.

We repeated the above procedure by using all possible combinations of monthly averaged data instead of the May–August season. Seasonal window lengths varied from 1 to 12 months, and the included months ranged from previous year September to current year September. We selected the May–August season for both annually varying and mean climate data, as this pair of seasons explained the most variance in formula (2). Choosing this season does not mean that other months of the previous or current year do not influence growth and, as such, climate sensitivity (see Babst et al., 2012, 2013).

Regression coefficients were calculated over the 1910–2009 period as well as over two independent periods 1910–1959 and 1960–2009. For the two independent periods $\overline{T_i^{\text{clim}}}$ was calculated over the respective 50 years. All regression slopes and R^2 values are based on robust regression with iteratively reweighted inverse least squares to dampen the effect of outliers in the rather small and heterogeneous data set. Because the high-pass filtered ABI time series are dimensionless, the obtained regression slopes reflect sensitivities of ABI to climate variation relative to a mean of one. Assuming a constant of proportionality (i.e., variance scales with mean growth rate) these relative sensitivities (expressed in percent per degree Celsius change) can be transposed to absolute sensitivities (in gram carbon per degree Celsius change) by multiplying the dimensionless time series with, for example, the observed mean ABI across the 49 sites of 233.5 g C m^{-2} $year^{-1}$.

We tested the robustness of our results by recalculating the plot chronologies following a more common dendrochronological method (hereafter termed *classic*). In this classic method raw ring widths of individual tree cores were first detrended with a cubic smoothing spline with a 50% frequency cutoff at 10 years and then averaged to a mean plot chronology using a biweight robust mean and variance stabilization to account for changing sampling replication over time (Frank et al., 2007). The main difference to the ABI chronology development is that in the classic dendrochronological approach all samples have the same weight, whereas trees that grow the fastest—usually the biggest—dominate the ABI chronology. We applied this alternative classic approach to our data and compared these results to those derived of a much larger tree ring network standardized accordingly (992 sites, Babst et al., 2013). Climate sensitivities were calculated in the same way as described above.

2.5. Dynamic Global Vegetation Models

Analogous to the ABI series, we assessed the climate sensitivity of annual NPP estimated from a suite of 11 process-based vegetation models for the 1910–2009 period across the entire grid of Europe (32–70°N, −10 to 30°E). The 11 models include 8 DGVMs of the TRENDY model intercomparison project (http://dgvm.ceh.ac.uk; Sitch et al., 2015) and 2 models previously used for comparisons with tree ring width chronologies over a set of 992 locations across Europe, hereafter called GEB-ORCHIDEE, GEB-LPJ (Babst et al., 2013), and LPX-Bern v1.2 (Table S3). The two GEB models were restricted to model only tree plant functional types (PFT), whereas all other models simulated all PFT. All models were forced with the observed change in atmospheric CO_2 concentration, historical climate change, and land use being held constant (representing the S2 scenario of the TRENDY project).

Modeled ABI outputs are neither reported in the TRENDY project database nor in the GEB models. However, based on very high correlation between detrended modeled ABI and NPP time series in the LPX model (median correlation of all grid cells: $r = 0.95$; Figure S2), we conclude that it is appropriate to compare measured ABI with modeled NPP. Although there are many approaches to model carbon allocation (Franklin et al., 2012) most DGVMs and in particular all other models evaluated here use similar allometric carbon allocation relationships as LPX and hence we assume similar relationships between modeled ABI and NPP in the other DGVMs. Inferences drawn from general relationships between measured ABI and modeled NPP behavior should thus be largely independent of the actual selected model output (but see also discussion section 4.2).

3. Results

3.1. Tree Ring-Based Mean ABI and Interannual Variability

The observed mean site ABI ranges from 75 to 540 g C m^{-2} $year^{-1}$ over 1980–2009. Assuming that ABI is an ~30–50% fraction of NPP (Babst, Bouriaud, Papale, et al., 2014), our observed network mean ABI of

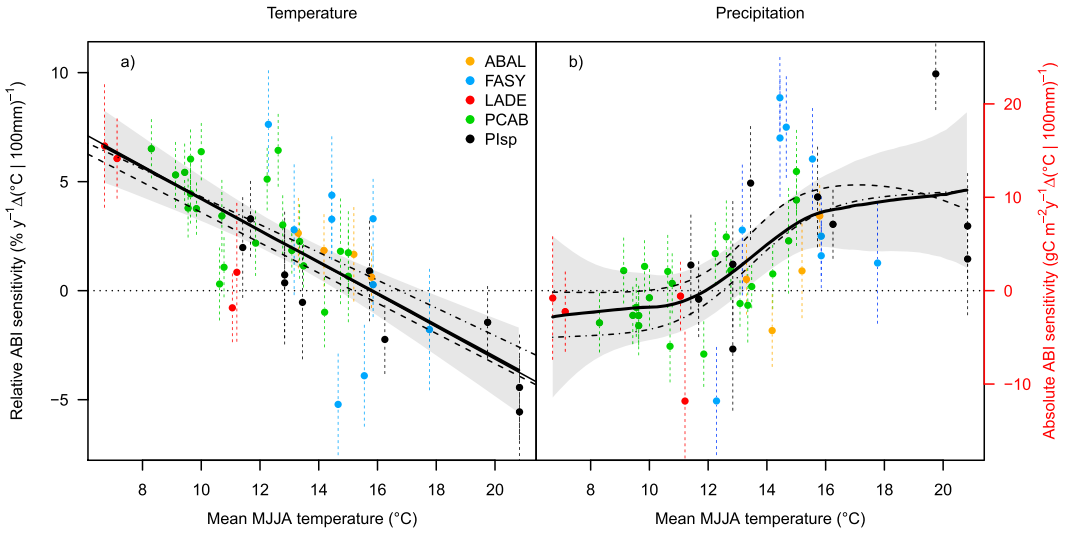

Figure 2. Relative (left-hand black *y* axis) and absolute (right-hand red *y* axis) sensitivities of ABI to a change of 1 °C in MJJA temperature (a) and 100 mm of MJJA precipitation (b). Data are plotted against average MJJA temperature over the 1910–2009 period. All time series were high-pass filtered with a cubic smoothing spline (50% frequency cutoff at 10 years, left-hand axis units) and subsequently multiplied by the network mean ABI of 233.5 g C m^{-2} year^{-1} (right-hand axis units). Colors refer to different dominant species as in Figure 1. Vertical dotted lines show the standard error of each sensitivity estimate. The black line represents the regression line based on robust linear regression (a) or based on general additive model including a smoothing term (b); gray shading indicates the 95% confidence interval after 1,000 simulations accounting for uncertainties in the sensitivity values. Dashed (dash-dotted) lines show the regression line of the 1910–1959 (1960–2009) period. The early split period regression lines are based on the sensitivities of 45 plots against the mean MJJA temperature of the 1910–1959 period. The late period regression lines show the regression of all plot sensitivities against mean MJJA temperature of the 1960–2009 period. MJJA = May, June, July, August; ABI = aboveground biomass increment.

233.5 ± 111 g C m^{-2} year^{-1} overlaps with the inventory-based mean NPP (447 ± 112 g C m^{-2} year^{-1}) of Europe (Luyssaert et al., 2010). Controlled for species, the within-site standard deviation of individual trees increases proportionally to mean ABI (see data from three exemplary *Picea abies* plots in Figure 1c). For each of the four most represented species *Picea abies*, *Fagus sylvatica*, *Pinus sylvestris*, and *Larix decidua*, the coefficient of determination of this relationship is above 0.95. For the highest replicated tree species *Picea abies* the average coefficient of variation of individual trees is 23.7 and ranges from 15.9 to 31.6 as a function of increasing mean May–August temperature ($R^2 = 0.45$, $p < 0.001$, $N = 29$, Figure 1d).

The relationship between standard deviation and growth level is also proportional between sites ($R^2 = 0.78$, $p < 0.001$) with an average coefficient of variation of 15.3 ± 4.4% (Figure 1e). Concordant with the individual tree-based analysis, our data show a similarly strong and statistically significant positive relationship between stand level coefficient of variation and mean May–August temperature ($R^2 = 0.55$, $p < 0.001$, $N = 22$) for the *Picea abies* dominated stands.

3.2. Tree Ring-Derived Climate Sensitivity

We find that temperature sensitivity, s_i^T, strongly depends on mean May–August temperature ($R^2 = 0.64$, $p < 0.001$, Figure 2a) and ranges from +7.6% Δ°C^{-1} at a high-elevation *Fagus sylvatica* site to −5.6% Δ°C^{-1} at the warmest site (*Pinus pinaster*). Across the range of observed temperatures and sites, temperature sensitivity changes by −0.72% per degree Celsius increase in mean May–August temperature. Notably, these results indicate a threshold temperature of 15.9 ± 1.4 °C above (below) which forest growth decreases (increases) with warming. This mean May–August temperature-dependent relationship stays temporally stable between the first and second halves of the twentieth century. The effect of minor data loss in the early period (only 36 of the 49 plots span the full 1910–2009 period, Table S1) does not affect this conclusion (Figure S3). A similar but curvilinear and weaker relationship is observed for precipitation ($R^2 = 0.44$, $p < 0.001$, Figure 2b). Because of the above-described spread versus level relationship, we can multiply the dimensionless time series with, for example, the network mean ABI of 233.5 g C m^{-2} year^{-1} and translate the relative sensitivities into absolute sensitivities (secondary *y* axis of Figure 2).

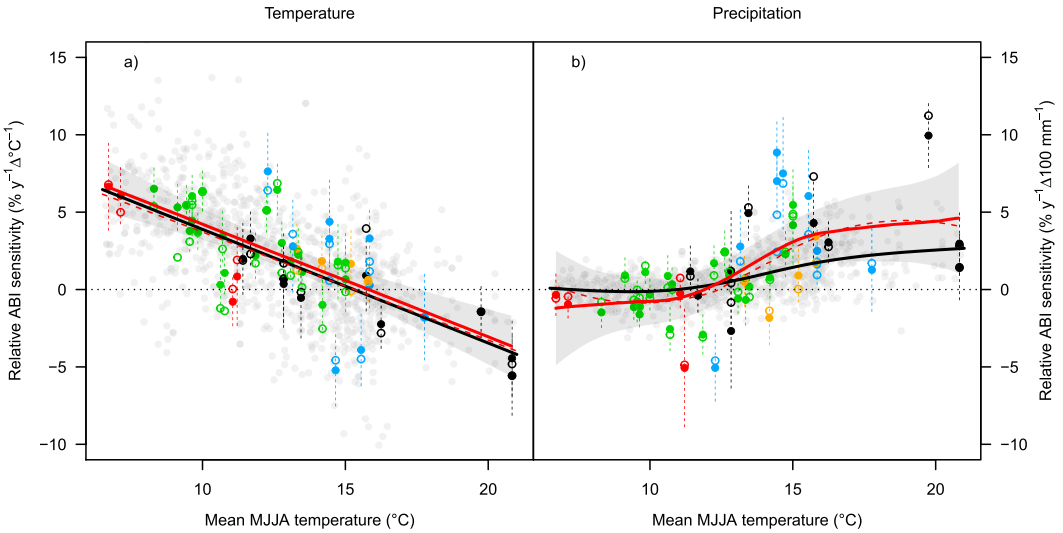

Figure 3. Relative sensitivities between the 992 tree ring chronologies from Babst et al. (2013, gray dots) and MJJA temperature (a) and precipitation (b) plotted against mean MJJA temperature. Colored circles represent the regression coefficients of the 49 biomass plots of this study. Filled points, vertical dotted lines, and solid red line represent the sensitivities, uncertainties, and regression line as shown in Figure 2; empty circles and dashed red line represent sensitivities and the regression line derived from the classic chronology development approach. The black regression line refers to Babst et al. (2013). All sensitivities are based on the 10-year high-pass filtered data. MJJA = May, June, July, August; ABI = aboveground biomass increment.

Our observed climate sensitivity patterns are unaffected by the choice of how the plot chronologies are calculated (Figure 3). In 48 of the 49 plots the sensitivity estimates of the classic approach (i.e., first detrending of individual time series and subsequent averaging, thus giving the same weight to each tree and sample irrespective of the tree's absolute growth increment) lie within the uncertainty of the initial sensitivity estimates from the ABI chronologies. This allows us to compare the climate sensitivities derived from our new tree ring network with the much larger data set of Babst et al. (2013). Even though most of our plots are located in Switzerland (23 of 49), the threshold temperature and magnitude of temperature sensitivities of the new network are undistinguishable from the relationship derived from 992 classically established chronologies (i.e., which are predominantly built of only dominant trees) that are much more evenly distributed across Europe. We want to stress that both networks do not sufficiently cover tree species of the warm and water-limited Mediterranean region and as such predominantly represent the climate sensitivity gradient of temperate and boreal species of Central and Northern Europe.

3.3. Climate Sensitivity of Vegetation Models

The DGVM ensemble reveals substantial spread in the coefficients of variation of modeled NPP, which on average are lower than the observed ABI coefficients of variation (Figure 1f). In contrast to the observational data, 7 out of 11 models show a local minimum in relative interannual variability (range: 3.8–12.1%) at intermediate temperatures (10–13.3 °C mean May–August temperature). Furthermore, response slopes and temperature thresholds of the individual ensemble members diverge strongly (Figure 4). Nine out of 11 models exceed the observed slope by up to 3 times, and a wide spread of 11.2–18.9 °C (with outliers of 25.0 and 26.7 °C, Figures 4a and 4b) emerged for the threshold temperatures. Despite this spread, the ensemble mean threshold temperature of 15.7 ± 0.7 °C (Figure 4b) agrees well with our tree ring-based estimate, although the average response slope is steeper (−1.1% Δ°C, Figure 4c).

Further examination of the results demonstrates that the DGVMs are excessively sensitive to both temperature and precipitation variability (Figures 5–7). Compared to ABI, the models show stronger positive (negative) temperature sensitivity at low (high) mean May–August temperature (Figures 5 and 6). Furthermore, the common low precipitation sensitivity in both the observations and models at cooler mean May–August temperature (range: −0.9% to 4.1% Δ100 mm^{-1}) becomes too strongly positive in the models above 16.6 °C (ABI: 2.2% Δ100 mm^{-1}; model mean: 13.3% Δ100 mm^{-1}, Figures 5 and 7). Lastly, we observe an

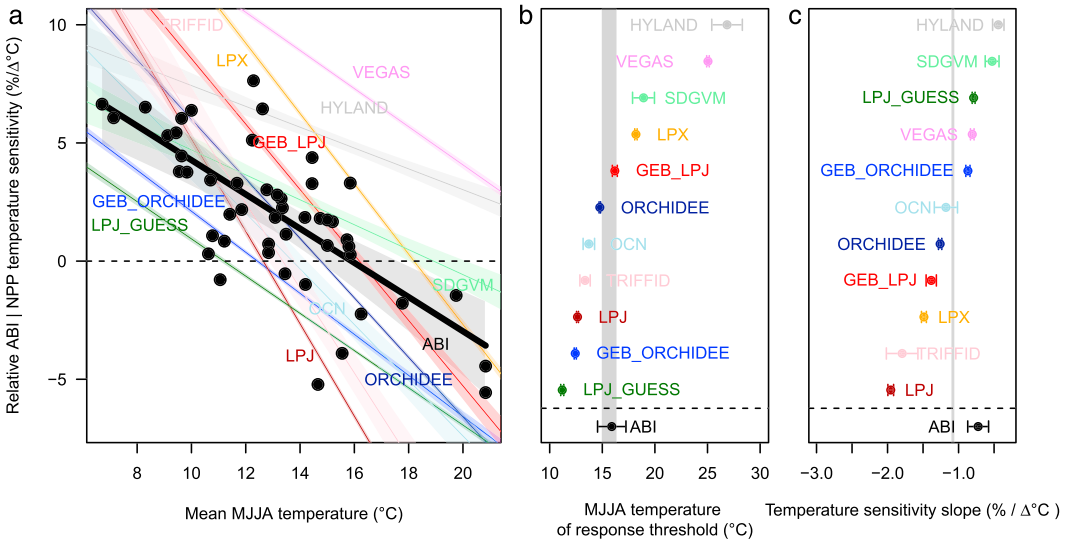

Figure 4. Relative temperature sensitivities of observed ABI and modeled NPP. The straight lines in (a) are based on robust linear regressions with shaded areas denoting the 95% confidence interval. The gray bars in (b) and (c) show the aggregate model mean response threshold and average temperature sensitivity slope, respectively, with uncertainties (95% confidence interval). Model values are derived using the entire grid of Europe. ABI = aboveground biomass increment; NPP = Net Primary Productivity; MJJA = May, June, July, August.

increase in model ensemble spread with higher mean May–August temperature, which is exceptionally prominent for precipitation sensitivity with a 4% sensitivity spread below 10 °C and 33% above 16.6 °C (Figure 5). These tendencies, observed for the European-wide gridded analyses, also hold when focusing only on grid cells that correspond to the tree ring sites (Figure S4). Model runs restricted to model only tree PFT showed better model-observation agreement compared to their all-PFT equivalents (Table S4 and Figures 6 and 7), yet the abundance of PFTs believed to be more climatically sensitive (i.e., C3 grasses) is not sufficient to explain the discrepancies between models and observations (Figure S5).

4. Discussion

Considerable effort over the past decade has been devoted to constraining the climate sensitivity of the terrestrial carbon cycle. Such investigations have typically been either spatially highly resolved with relative sensitivities inferred from correlations between ecosystem processes and climate parameters (Beer et al., 2010; Jung et al., 2017; Nemani, 2003; Piao et al., 2014) or alternatively, the absolute climate sensitivity has been estimated from variation in atmospheric CO_2 concentrations across large spatial domains and variability within biomes left unaddressed (Ahlström et al., 2015; Ciais et al., 2014; Cox et al., 2013). In the present study, we combine elements of both of these approaches—made possible with a biomass-oriented tree ring sampling design (Babst, Bouriaud, Alexander, et al., 2014; Nehrbass-Ahles et al., 2014)—to provide spatially constrained estimates of climate sensitivity for European forest ABI to benchmark DGVM performance.

4.1. Spatial Uncertainties

We demonstrate high variability in the magnitude and even the sign of the climate sensitivity of ABI or NPP, depending upon the specific location of a site within the focal biome. Our empirical patterns show that European forests south of ~50°N (excluding the Alps and representing roughly 53% of the CRU land grid cells) will suffer from rising temperatures and simultaneously benefit from more precipitation and an increase in water balance. While the mean model response reflects our climate sensitivity observations reasonably well, we note that individual models show a diverse picture of regions where NPP is enhanced or reduced by short-term climate variations (Figures 5 and 6). For example, VEGAS simulates positive effects of warmer growing season temperature on NPP as far south as 40°N, whereas LPJ predicts already negative effects of warmer temperatures south of 58°N. Model predictions are least certain for the highly productive and intensely managed regions in temperate Europe (mean May–August temperature: 13–16 °C, roughly

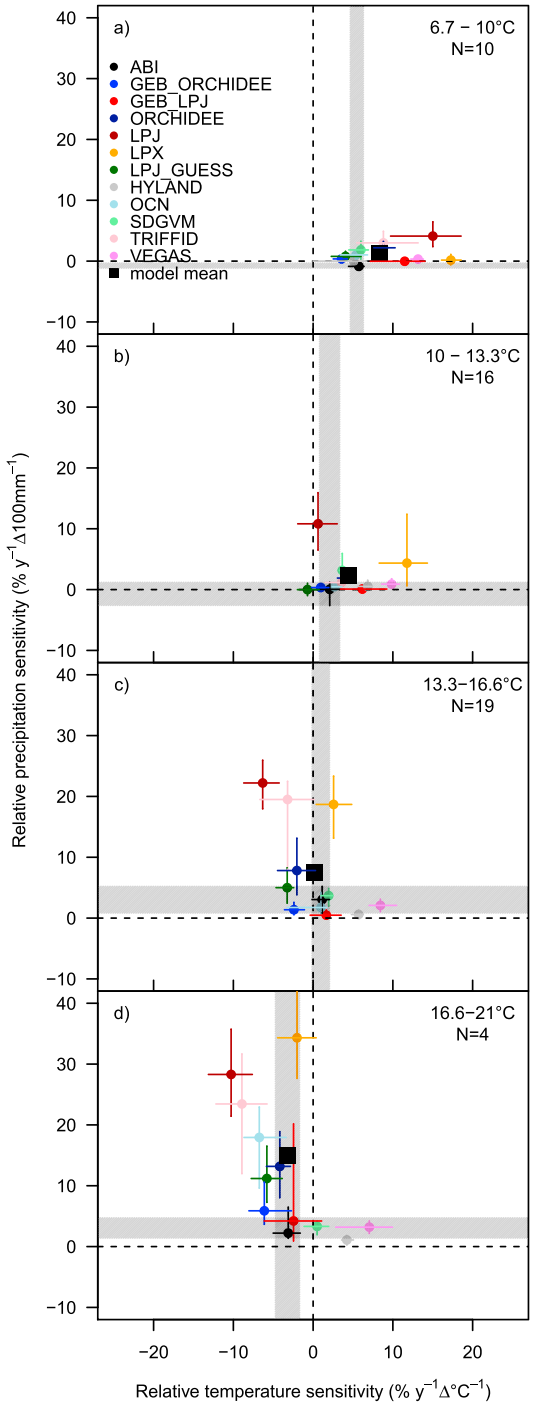

Figure 5. Bivariate plot of climate sensitivities of the ABI chronologies and 11 DGVMs binned into four temperature range classes. Each panel represents a MJJA mean temperature range class, given in the upper right corner of each panel, and includes locations from cold (a) to warm (d) regions. *N* represents the number of biomass plots in the given temperature range. Points represent the median sensitivity, while horizontal and vertical lines through the points represent the interquartile ranges. The gray shaded area outlines the interquartile range of ABI derived sensitivity estimates, and the black square shows the mean response of the 11 DGVMs. ABI = aboveground biomass increment; DGVM = dynamic global vegetation model; MJJA = May, June, July, August.

equivalent to the latitudinal band of 46–58°N), suggesting that reductions in model uncertainties will be required to more effectively guide silvicultural practices (Lindner et al., 2014).

4.2. Assessing Climate Sensitivity

Assessing the climate sensitivity of forest productivity and comparing it to DGVM estimates is a challenging endeavor. While this comparison was undertaken using the two most closely related metrics that can be derived from the tree ring data and the archived TRENDY simulations (Sitch et al., 2015), in the following section, we assess possible caveats of both data sources and their comparison, particularly with respect to our main conclusion that the models overestimate the climate sensitivity.

4.2.1. Tree Ring Sensitivities

Although the replication of our data set decreases toward the warmest and coolest mean May–August temperature, our observed sensitivities concur with a much larger tree ring data set spanning the whole of Europe (Babst et al., 2013). Our findings further confirm general theory about climate-driven tree growth mechanisms (Fritts, 1976), where at cool locations interannual growth variability is primarily driven by growing season temperatures and at warm locations precipitation and temperature play a more equally important role. However, rather than showing only correlation coefficients that only report sign and level of noise of the relationship between tree growth and climate as usually done in large tree ring network analyses (Babst et al., 2013; St. George, 2014; Vicente-Serrano et al., 2014; Williams et al., 2010), we take into account the magnitude of interannual growth variability of the time series and report absolute sensitivities.

Traditionally, dendrochronologists have sampled only dominant and undamaged trees to reduce the number of samples needed to obtain a representative growth signal and to extend the time series as far back in time as possible. Nehrbass-Ahles et al. (2014), however, found that this classic approach is potentially unsuitable to infer trends and absolute levels of ABI, also because usually very few stand related metadata (such as stand density and standing basal area) are collected during the sampling. Despite these issues, however, they found that the interannual signal and climate-growth relationships after removing subdecadal to multidecadal frequencies (i.e., detrending with a flexible smoothing spline) are largely unaffected by the initial sampling design, which the recalculation of our plot chronologies confirms. Furthermore, the close match of the temperature sensitivity relationship of the Babst et al. (2013) network to our results validates the use of classically sampled tree ring chronologies and the classic averaging procedure for climate sensitivity analysis of the entire forest ecosystems in central and northern Europe. Whether this is true in other regions and continents needs to be evaluated, and one has to ensure that tree ring data are a representative subset of the investigated forest ecosystem if used for addressing broad-scale ecological questions. Furthermore, samples should be recently enough collected to be compared with data from other carbon cycle data streams (Babst et al., 2017). The advantage of our sampling strategy and chronology calculation is that individual ABI time series are weighted according to each tree's absolute growth increment, and we can directly calculate ABI without the need to be close to forest inventory plots. However, the observed similarities between the ABI and classic

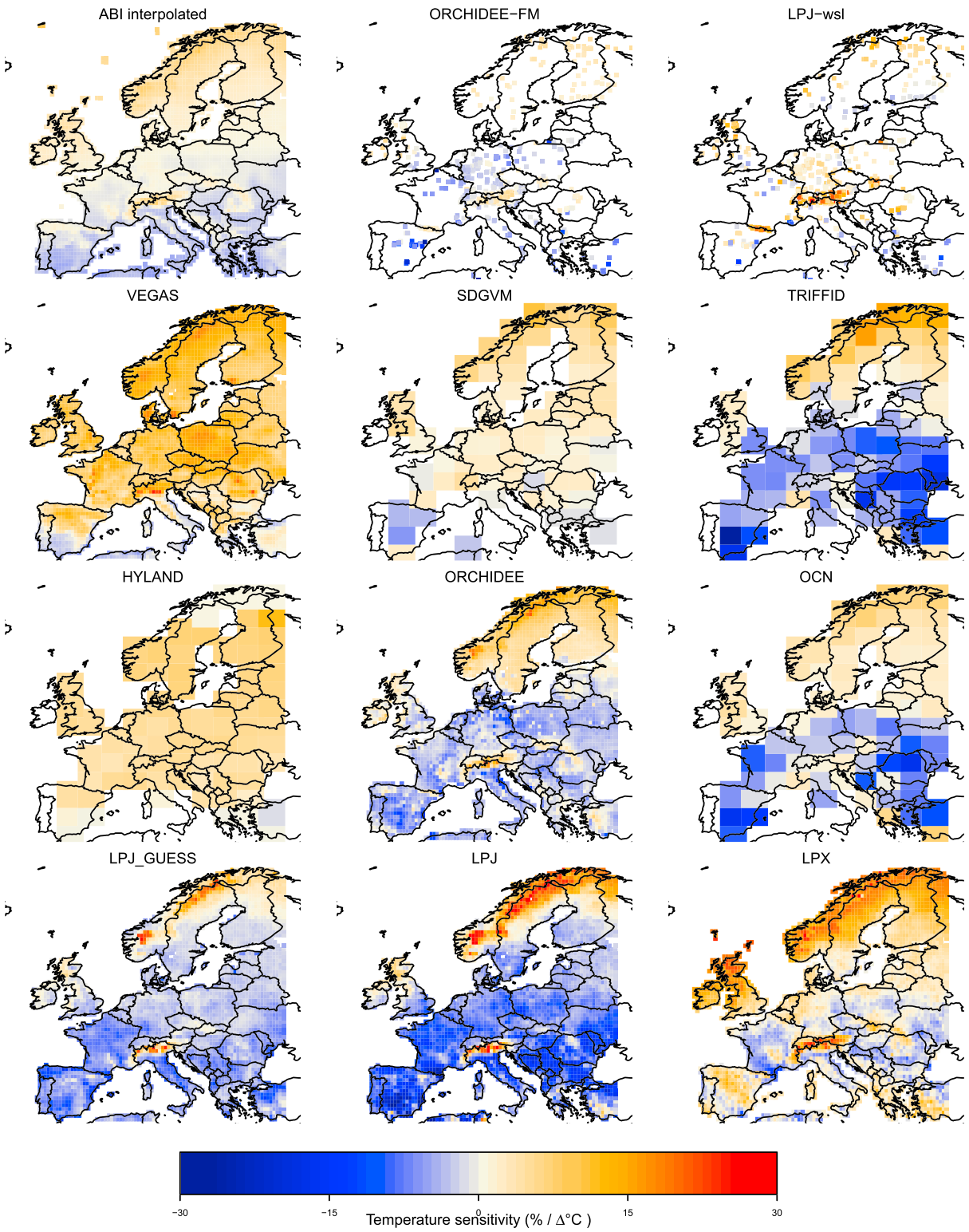

Figure 6. Tree ring derived (ABI) and modeled (NPP) temperature sensitivity map. Top left shows extrapolated temperature sensitivity of ABI via regression of Figure 2a. Model sensitivities are actual values. ABI = aboveground biomass increment; NPP = Net Primary Productivity.

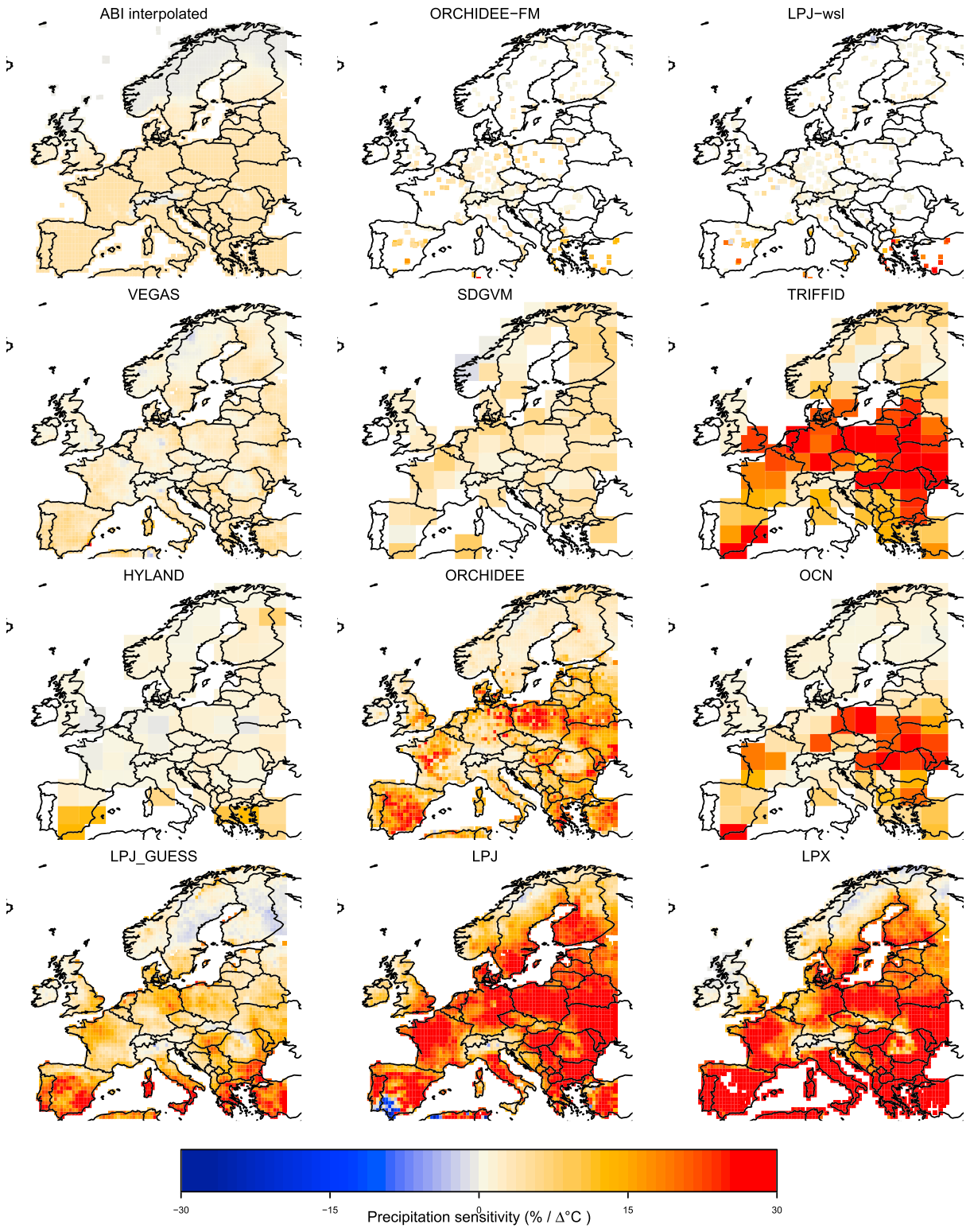

Figure 7. Tree ring derived (ABI) and modeled (NPP) precipitation sensitivity map. Top left shows extrapolated precipitation sensitivity of ABI via regression of Figure 2b. Model sensitivities are actual values. ABI = aboveground biomass increment; NPP = Net Primary Productivity.

approach in our study might stem from the rather simple stand composition of most of our ABI plots (in 35 of 49 plots 75% of plot basal area comprises one species) that does not lead to a clear signal dampening, which has been observed in mixed species stands where the most abundant species contributes to less than 40% of plot basal area (Teets et al., 2018).

By transforming tree ring data with allometric equations, we assume a proportional growth response to climate variability along the stem. There is limited evidence that, despite a very high correlation, radial growth in poor growth years is more reduced at 1.30 m (the usual height for tree ring sampling) than in samples taken near the tree's crown, possibly leading to overestimated ABI sensitivity (Bouriaud et al., 2005; van der Maaten-Theunissen & Bouriaud, 2012). On the other hand, our empirical measures might underestimate the actual climate sensitivity of NPP, as current year's ABI is partly composed of previous year's stored carbohydrates. Natural and anthropogenic disturbances might further dampen the climate signal, and long-term effects of climate variation, nutrient, and CO_2 fertilization on absolute tree growth are not evaluated herein.

However, uncertainties related to the above mentioned caveats, such as tree allometry, sampling design, and chronology development approach, on the interannual growth signal appear small in light of extensive replication and spatial distribution of publicly available tree ring data sets (such as the International Tree Ring Data Base; https://www.ncdc.noaa.gov/paleo-search/) and spatial homogeneity of year-to-year growth variability (Babst et al., 2012; Charney et al., 2016; Williams et al., 2013) that make tree rings a valuable annually resolved and in situ data source of aboveground woody NPP variability (Dye et al., 2016).

4.2.2. DGVM Sensitivities

The enhanced climate sensitivity of NPP from DGVMs has been previously reported (Babst et al., 2013; Ciais et al., 2014; Huang et al., 2016; Piao et al., 2013; Rollinson et al., 2017; Zhang et al., 2017) and may result from inadequate model parameterizations related to soil moisture availability and plant water transport. Circularity issues introduced by correlating NPP with the same climate data that initially drove the model (Babst et al., 2013) may further contribute to increased climate sensitivity. Most models presently vary carbon allocation among living tissue pools (i.e., roots, sapwood, and foliage) depending upon climatic stressors and plant functional constraints based on simple allometric relationships (cf. supporting information Table S1 in Sitch et al., 2015). The allocation schemes are based upon empirical evidence that proportions of forest biomass allocation change, for example, between dry and wet regions on Earth (Reich et al., 2014). Yet the degree to which allocation to the different tissues, at a regional scale, actually varies interannually is poorly understood. The lack of long-term interannual data of root growth and foliage production highlights the need for research on interannual variability of carbon allocation in mature forests. After the installation of Level II intensive monitoring plots (UNECE ICP Forests Network) in the mid-1990s, litter fall data (representing leaf and fruit production) now reach sufficient length to robustly analyze the relationships between climate, aboveground woody biomass increment, and foliage production. This should ultimately lead to improved representation of annual variability in the (currently simplified) allocation formulations in DGVMs.

We are aware that the temporal behavior of total NPP and aboveground woody NPP (our ABI) is not identical, although appears tightly correlated in extratropical forests (Figure S1). Yet a direct comparison between tree ring data and modeled sapwood increment (i.e., the part of NPP attributed to new wood tissue) of the LPX model does not lead to different conclusions. In fact, it increases the model-observation discrepancy (Figure S6) as the interannual variability of modeled sapwood increment (median coefficient of variation: 33%) is nearly 3 times the variability of NPP (13%) and both time series are highly correlated (r = 0.95, averaged over all grid cells). Although sapwood increment may be considered as the carbon pool that is most closely related to ABI, in LPX, this pool was never intended to mimic actual tree growth.

Another reason for the observation-model sensitivity discrepancy might be that nonstructural carbohydrates (frequently described as the carbon reserve pool) are not represented in most state-of-the-art DGVMs. This factor may help explain the high sensitivity to current year's growing season climate of the models and is demonstrated by (i) significantly different autocorrelative properties of modeled and observed time series (Figure S7), (ii) lower ecosystem persistence in models (Pappas et al., 2017), (iii) the rather immediate NPP recovery after climate extremes compared to that of tree ring observations (Anderegg et al., 2015), and (iv) missing lag effects of modeled NPP time series compared to observed tree ring widths (Zhang et al., 2017).

5. Conclusions

Our study provides the first long-term empirical estimates for threshold temperatures between positive and negative responses of European forests to warming and the associated increase in evaporative demand. European forests with mean May–August temperature above 15.9 ± 1.4 °C (~9 °C mean annual temperature) are subject to growth decline with further warming and concurrent increases in moisture stress. Future investigations are warranted to determine if this threshold temperature and the magnitude of changing climate sensitivity with changing mean temperature is similar in other parts and other species of the world. Coupled Earth-system models represent the best available tool to assess how these interactions may change in the future, yet they require accurate representation of ecosystem responses to interannual climate variation. We have shown that the DGVM ensemble median reflects well the observed empirical responses. However, the large spread of individual ensemble members indicates substantial uncertainties regarding key ecosystem processes and the importance of multimodel assessments. Ongoing modeling efforts, for example, considering carbon reserve pools and remobilization of nonstructural carbohydrates in DGVMs through the implementation of carbon allocation schemes reflecting actual phenological phases (yet awaiting globally useful generalizations, Gea-Izquierdo et al., 2015), or refining the representation of stem wood carbon by explicitly simulating tree rings (Li et al., 2014), will further increase the relevance of our empirical ABI benchmarks.

We find that climate sensitivities of ABI vary in tight connection to the ambient climatic conditions with values ranging from −5.6% to 7.6% $\Delta°C^{-1}$ across the network. These observations question the relevance of a single large-scale estimate for the climate sensitivity of the terrestrial carbon cycle (or mean values of smaller units thereof, Ahlström et al., 2015; Ciais et al., 2014; Cox et al., 2013) and suggest that more research is required on transient behavior of individual biome responses to climate variation.

Acknowledgments
The authors would like to thank the TRENDY project members for sharing their data and Richard Peters, Kristina Seftigen, and Jesper Björklund for discussion. Additional thanks to Lenka Mateju and Katarzyna Czober and everyone who was involved in the extensive and intensive field work and lab work. F. B. acknowledges funding from the Swiss National Science Foundation (P300P2_154543) and the EU Horizon-2020 project *BACI* (grant 640176). S. K., F. J., R. S., and D. C. F. are supported by the SNF iTREE sinergia project 136295. F. J., S.L., and R. S. acknowledge support by the Swiss National Science Foundation (200020_172476), O. B. acknowledges funding from UEFISCDI project PN-II-ID-PCE-2011-3-07, and V. T. is supported by the GACR 15-14840S and CIGA 20154316. Tree ring data are publicly available under https://www.bgc-jena.mpg.de/geodb/projects/Data.php and selecting the BACI project. The authors declare no conflict of interest.

References

Ahlström, A., Raupach, M. R., Schurgers, G., Smith, B., Arneth, A., Jung, M., et al. (2015). The dominant role of semi-arid ecosystems in the trend and variability of the land CO_2 sink. *Science*, *348*(6237), 895–899. https://doi.org/10.1126/science.aaa1668

Anderegg, W. R. L., Schwalm, C., Biondi, F., Camarero, J. J., Koch, G., Litvak, M., et al. (2015). Pervasive drought legacies in forest ecosystems and their implications for carbon cycle models. *Science*, *349*(6247), 528–532. https://doi.org/10.1126/science.aab1833

Babst, F., Bouriaud, O., Alexander, R., Trouet, V., & Frank, D. (2014). Toward consistent measurements of carbon accumulation: A multi-site assessment of biomass and basal area increment across Europe. *Dendrochronologia*, *32*(2), 153–161. https://doi.org/10.1016/j.dendro.2014.01.002

Babst, F., Bouriaud, O., Papale, D., Gielen, B., Janssens, I. A., Nikinmaa, E., et al. (2014). Above-ground woody carbon sequestration measured from tree rings is coherent with net ecosystem productivity at five eddy-covariance sites. *New Phytologist*, *201*(4), 1289–1303. https://doi.org/10.1111/nph.12589

Babst, F., Carrer, M., Poulter, B., Urbinati, C., Neuwirth, B., & Frank, D. (2012). 500 years of regional forest growth variability and links to climatic extreme events in Europe. *Environmental Research Letters*, *7*(4), 045705. https://doi.org/10.1088/1748-9326/7/4/045705

Babst, F., Poulter, B., Bodesheim, P., Mahecha, M. D., & Frank, D. C. (2017). Improved tree-ring archives will support Earth-system science. *Nature Ecology & Evolution*, *1*(2), 0008. https://doi.org/10.1038/s41559-016-0008

Babst, F., Poulter, B., Trouet, V., Tan, K., Neuwirth, B., Wilson, R., et al. (2013). Site- and species-specific responses of forest growth to climate across the European continent. *Global Ecology and Biogeography*, *22*(6), 706–717. https://doi.org/10.1111/geb.12023

Beer, C., Reichstein, M., Tomelleri, E., Ciais, P., Jung, M., Carvalhais, N., et al. (2010). Terrestrial gross carbon dioxide uptake: Global distribution and covariation with climate. *Science*, *329*(5993), 834–838. https://doi.org/10.1126/science.1184984

Bouriaud, O., Bréda, N., Dupouey, J.-L., & Granier, A. (2005). Is ring width a reliable proxy for stem-biomass increment? A case study in European beech. *Canadian Journal of Forest Research*, *35*(12), 2920–2933. https://doi.org/10.1139/x05-202

Charney, N. D., Babst, F., Poulter, B., Record, S., Trouet, V. M., Frank, D., et al. (2016). Observed forest sensitivity to climate implies large changes in 21st century North American forest growth. *Ecology Letters*, *19*(9), 1119–1128. https://doi.org/10.1111/ele.12650

Churkina, G., Schimel, D., Braswell, B. H., & Xiao, X. (2005). Spatial analysis of growing season length control over net ecosystem exchange. *Global Change Biology*, *11*(10), 1777–1787. https://doi.org/10.1111/j.1365-2486.2005.001012.x

Ciais, P., Sabine, C., Bala, G., Bopp, L., Brovkin, V., Canadell, J., et al. (2014). Carbon and other biogeochemical cycles. In *Climate change 2013: the physical science basis. Contribution of Working Group I to the Fifth Assessment Report of the Intergovernmental Panel on Climate Change* (pp. 465–570). Cambridge University Press. Retrieved from http://pubman.mpdl.mpg.de/pubman/item/escidoc:2058766/component/escidoc:2058768/WG1AR5_Chapter06_FINAL.pdf

Clark, D. A., Brown, S., Kicklighter, D. W., Chambers, J. Q., Thomlinson, J. R., & Ni, J. (2001). Measuring net primary production in forests: Concepts and field methods. *Ecological Applications*, *11*(2), 356–370. https://doi.org/10.1890/1051-0761(2001)011[0356:MNPPIF]2.0.CO;2

Cox, P. M., Pearson, D., Booth, B. B., Friedlingstein, P., Huntingford, C., Jones, C. D., & Luke, C. M. (2013). Sensitivity of tropical carbon to climate change constrained by carbon dioxide variability. *Nature*, *494*(7437), 341–344. https://doi.org/10.1038/nature11882

Davis, S. C., Hessl, A. E., Scott, C. J., Adams, M. B., & Thomas, R. B. (2009). Forest carbon sequestration changes in response to timber harvest. *Forest Ecology and Management*, *258*(9), 2101–2109. https://doi.org/10.1016/j.foreco.2009.08.009

Dye, A., Barker Plotkin, A., Bishop, D., Pederson, N., Poulter, B., & Hessl, A. (2016). Comparing tree-ring and permanent plot estimates of aboveground net primary production in three eastern U.S. forests. *Ecosphere*, *7*(9), e01454. https://doi.org/10.1002/ecs2.1454

Fatichi, S., Leuzinger, S., & Körner, C. (2014). Moving beyond photosynthesis: From carbon source to sink-driven vegetation modeling. *New Phytologist*, *201*(4), 1086–1095. https://doi.org/10.1111/nph.12614

Foster, J. R., D'Amato, A. W., & Bradford, J. B. (2014). Looking for age-related growth decline in natural forests: Unexpected biomass patterns from tree rings and simulated mortality. *Oecologia*, *175*(1), 363–374. https://doi.org/10.1007/s00442-014-2881-2

Frank, D., Esper, J., & Cook, E. R. (2007). Adjustment for proxy number and coherence in a large-scale temperature reconstruction. *Geophysical Research Letters*, *34*, L16709. https://doi.org/10.1029/2007GL030571

Franklin, O., Johansson, J., Dewar, R. C., Dieckmann, U., McMurtrie, R. E., Brännström, Å., & Dybzinski, R. (2012). Modeling carbon allocation in trees: A search for principles. *Tree Physiology*, *32*(6), 648–666. https://doi.org/10.1093/treephys/tpr138

Fritts, H. (1976). *Tree Rings and Climate*. Elsevier.

Gea-Izquierdo, G., Guibal, F., Joffre, R., Ourcival, J. M., Simioni, G., & Guiot, J. (2015). Modelling the climatic drivers determining photosynthesis and carbon allocation in evergreen Mediterranean forests using multiproxy long time series. *Biogeosciences*, *12*(12), 3695–3712. https://doi.org/10.5194/bg-12-3695-2015

Harris, I., Jones, P. D., Osborn, T. J., & Lister, D. H. (2014). Updated high-resolution grids of monthly climatic observations—The CRU TS3.10 dataset. *International Journal of Climatology*, *34*(3), 623–642. https://doi.org/10.1002/joc.3711

Hijmans, R. J., Cameron, S. E., Parra, J. L., Jones, P. G., & Jarvis, A. (2005). Very high resolution interpolated climate surfaces for global land areas. *International Journal of Climatology*, *25*(15), 1965–1978. https://doi.org/10.1002/joc.1276

Huang, Y., Gerber, S., Huang, T., & Lichstein, J. W. (2016). Evaluating the drought response of CMIP5 models using global gross primary productivity, leaf area, precipitation, and soil moisture data. *Global Biogeochemical Cycles*, *30*, 1827–1846. https://doi.org/10.1002/2016GB005480

Iversen, C., & Norby, R. (2014). Terrestrial plant productivity and carbon allocation in a changing climate. In B. Freedman (Ed.), *Global Environmental Change* (pp. 297–316). Dordrecht: Springer Netherlands. Retrieved from http://link.springer.com/10.1007/978-94-007-5784-4_2

Jung, M., Reichstein, M., Schwalm, C. R., Huntingford, C., Sitch, S., Ahlström, A., et al. (2017). Compensatory water effects link yearly global land CO_2 sink changes to temperature. *Nature*, *541*(7638), 516–520. https://doi.org/10.1038/nature20780

Le Quéré, C., Moriarty, R., Andrew, R. M., Peters, G. P., Ciais, P., Friedlingstein, P., et al. (2015). Global carbon budget 2014. *Earth System Science Data*, *7*(1), 47–85. https://doi.org/10.5194/essd-7-47-2015

Li, G., Harrison, S. P., Prentice, I. C., & Falster, D. (2014). Simulation of tree-ring widths with a model for primary production, carbon allocation, and growth. *Biogeosciences*, *11*(23), 6711–6724. https://doi.org/10.5194/bg-11-6711-2014

Lindner, M., Fitzgerald, J. B., Zimmermann, N. E., Reyer, C., Delzon, S., van der Maaten, E., et al. (2014). Climate change and European forests: What do we know, what are the uncertainties, and what are the implications for forest management? *Journal of Environmental Management*, *146*, 69–83. https://doi.org/10.1016/j.jenvman.2014.07.030

Luyssaert, S., Ciais, P., Piao, S. L., Schulze, E.-D., Jung, M., Zaehle, S., et al. (2010). The European carbon balance. Part 3: Forests. *Global Change Biology*, *16*(5), 1429–1450. https://doi.org/10.1111/j.1365-2486.2009.02056.x

Luyssaert, S., Inglima, I., Jung, M., Richardson, A. D., Reichstein, M., Papale, D., et al. (2007). CO_2 balance of boreal, temperate, and tropical forests derived from a global database. *Global Change Biology*, *13*(12), 2509–2537. https://doi.org/10.1111/j.1365-2486.2007.01439.x

Mauri, A., Strona, G., & San-Miguel-Ayanz, J. (2017). EU-forest, a high-resolution tree occurrence dataset for Europe. *Scientific Data*, *4*, 160123. https://doi.org/10.1038/sdata.2016.123

Medlyn, B. E., Zaehle, S., De Kauwe, M. G., Walker, A. P., Dietze, M. C., Hanson, P. J., et al. (2015). Using ecosystem experiments to improve vegetation models. *Nature Climate Change*, *5*(6), 528–534. https://doi.org/10.1038/nclimate2621

Nehrbass-Ahles, C., Babst, F., Klesse, S., Nötzli, M., Bouriaud, O., Neukom, R., et al. (2014). The influence of sampling design on tree-ring-based quantification of forest growth. *Global Change Biology*, *20*(9), 2867–2885. https://doi.org/10.1111/gcb.12599

Nemani, R. R. (2003). Climate-driven increases in global terrestrial net primary production from 1982 to 1999. *Science*, *300*(5625), 1560–1563. https://doi.org/10.1126/science.1082750

Noormets, A., Epron, D., Domec, J. C., McNulty, S. G., Fox, T., Sun, G., & King, J. S. (2015). Effects of forest management on productivity and carbon sequestration: A review and hypothesis. *Forest Ecology and Management*, *355*, 124–140. https://doi.org/10.1016/j.foreco.2015.05.019

Pappas, C., Frank, D. C., Koutsoyiannis, D., Babst, F., & Mahecha, M. D. (2017). Ecosystem functioning is enveloped by hydrometeorological variability. *Nature Ecology & Evolution*, *1*(9), 1263–1270. https://doi.org/10.1038/s41559-017-0277-5

Piao, S., Nan, H., Huntingford, C., Ciais, P., Friedlingstein, P., Sitch, S., et al. (2014). Evidence for a weakening relationship between interannual temperature variability and northern vegetation activity. *Nature Communications*, *5*(1), 5018. https://doi.org/10.1038/ncomms6018

Piao, S., Sitch, S., Ciais, P., Friedlingstein, P., Peylin, P., Wang, X., et al. (2013). Evaluation of terrestrial carbon cycle models for their response to climate variability and to CO2 trends. *Global Change Biology*, *19*(7), 2117–2132. https://doi.org/10.1111/gcb.12187

Poulter, B., Frank, D., Ciais, P., Myneni, R. B., Andela, N., Bi, J., et al. (2014). Contribution of semi-arid ecosystems to interannual variability of the global carbon cycle. *Nature*, *509*(7502), 600–603. https://doi.org/10.1038/nature13376

Reich, P. B., Luo, Y., Bradford, J. B., Poorter, H., Perry, C. H., & Oleksyn, J. (2014). Temperature drives global patterns in forest biomass distribution in leaves, stems, and roots. *Proceedings of the National Academy of Sciences*, *111*(38), 13,721–13,726. https://doi.org/10.1073/pnas.1216053111

Reichstein, M., Bahn, M., Ciais, P., Frank, D., Mahecha, M. D., Seneviratne, S. I., et al. (2013). Climate extremes and the carbon cycle. *Nature*, *500*(7462), 287–295. https://doi.org/10.1038/nature12350

Rollinson, C. R., Liu, Y., Raiho, A., Moore, D. J. P., McLachlan, J., Bishop, D. A., et al. (2017). Emergent climate and CO_2 sensitivities of net primary productivity in ecosystem models do not agree with empirical data in temperate forests of eastern North America. *Global Change Biology*, *23*(7), 2755–2767. https://doi.org/10.1111/gcb.13626

Rydval, M., Druckenbrod, D. L., Anchukaitis, K. J., & Wilson, R. J. S. (2015). Detection and removal of disturbance trends in tree-ring series for dendroclimatology. *Canadian Journal of Forest Research*, *46*(3), 387–401. https://doi.org/10.1139/cjfr-2015-0366

San-Miguel-Ayanz, J., de Rigo, D., Caudullo, G., Houston Durrant, T., & Mauri, A. (Eds.) (2016). *European Atlas of Forest Tree Species*. Luxembourg: Publication Office of the European Union.

Seidl, R., Schelhaas, M.-J., Rammer, W., & Verkerk, P. J. (2014). Increasing forest disturbances in Europe and their impact on carbon storage. *Nature Climate Change*, *4*(9), 806–810. https://doi.org/10.1038/nclimate2318

Sitch, S., Friedlingstein, P., Gruber, N., Jones, S. D., Murray-Tortarolo, G., Ahlström, A., et al. (2015). Recent trends and drivers of regional sources and sinks of carbon dioxide. *Biogeosciences*, *12*(3), 653–679. https://doi.org/10.5194/bg-12-653-2015

St. George, S. (2014). An overview of tree-ring width records across the Northern Hemisphere. *Quaternary Science Reviews*, *95*, 132–150. https://doi.org/10.1016/j.quascirev.2014.04.029

Teets, A., Fraver, S., Weiskittel, A. R., & Hollinger, D. Y. (2018). Quantifying climate–growth relationships at the stand level in a mature mixed-species conifer forest. *Global Change Biology*, *24*(8), 3587–3602. https://doi.org/10.1111/gcb.14120

van der Maaten-Theunissen, M., & Bouriaud, O. (2012). Climate–growth relationships at different stem heights in silver fir and Norway spruce. *Canadian Journal of Forest Research*, *42*(5), 958–969. https://doi.org/10.1139/x2012-046

Vicente-Serrano, S. M., Camarero, J. J., & Azorin-Molina, C. (2014). Diverse responses of forest growth to drought time-scales in the Northern Hemisphere. *Global Ecology and Biogeography*, *23*(9), 1019–1030. https://doi.org/10.1111/geb.12183

Wieder, W. R., Cleveland, C. C., Smith, W. K., & Todd-Brown, K. (2015). Future productivity and carbon storage limited by terrestrial nutrient availability. *Nature Geoscience*, *8*(6), 441–444. https://doi.org/10.1038/ngeo2413

Williams, A. P., Allen, C. D., Macalady, A. K., Griffin, D., Woodhouse, C. A., Meko, D. M., et al. (2013). Temperature as a potent driver of regional forest drought stress and tree mortality. *Nature Climate Change*, *3*(3), 292–297. https://doi.org/10.1038/nclimate1693

Williams, A. P., Michaelsen, J., Leavitt, S. W., & Still, C. J. (2010). Using tree rings to predict the response of tree growth to climate change in the continental United States during the twenty-first century. *Earth Interactions*, *14*(19), 1–20. https://doi.org/10.1175/2010EI362.1

Zhang, Z., Babst, F., Bellassen, V., Frank, D., Launois, T., Tan, K., et al. (2017). Converging climate sensitivities of European forests between observed radial tree growth and vegetation models. *Ecosystems*, *21*(3), 410–425. https://doi.org/10.1007/s10021-017-0157-5